Single-Walled Carbon Nanotubes of Controlled Diameter and Bundle Size and Their Field Emission Properties

Liang Zhang, Leandro Balzano, and Daniel E. Resasco*

School of Chemical, Biochemical, and Materials Engineering, University of Oklahoma, Norman, Oklahoma 73019

Received: March 2, 2005; In Final Form: June 8, 2005

Field emission studies were conducted on as-produced CoMoCAT single-walled carbon nanotube/silica composites with controlled nanotube diameter and bundle size. It has been observed that the as-produced nanotube material does not need to be separated from the high-surface area catalyst to be an effective electron emitter. By adjusting the catalytic synthesis conditions, single-walled carbon nanotubes (SWNT) of different diameters and bundle sizes were synthesized. A detailed characterization involving Raman spectroscopy, optical absorption (vis-NIR), SEM, and TEM was conducted to identify the nanotube species present in the different samples. The synthesis reaction temperature was found to affect the nanotube diameter and bundle size in opposite ways; that is, as the synthesis temperature increased the nanotube average diameter became larger, but the bundle size became smaller. A gradual and consistent reduction in the emission onset field was observed as the synthesis temperature increased. It is suggested that the bundle size, more than the nanotube diameter or chirality, determines the field emission characteristics of these composites. This is a clear demonstration that field emission characteristics of SWNT can be controlled by the nanotube synthesis conditions.

Introduction

During the past few years, single-walled carbon nanotubes have generated much interest because of their unique structure and properties. It is widely accepted that one of their potential applications might be in field emission devices.[1−4] Among the numerous studies dedicated to nanotube field emitters, great attention has been paid to optimizing the techniques for practical and reliable device fabrication.[5−14] In more fundamental studies, the mechanisms of field-induced electron emission, as well as the relationship between the nanotube structural parameters and emission properties, have been the focus of many publications.[1,12,15−18] What makes SWNTs good candidates for field emitters is the combination of their natural geometry, chemical stability, and electrical characteristics. They could be used as the electron source in a whole range of devices, including flat panel displays, light elements, e-beam sources for lithography, and so forth. Among these applications, field emission displays (FEDs) have attracted significant attention as they could become one of the first commercial products using nanotubes. In 1999, Choi et al.[19] built the first SWNT-based FED at Samsung. Carbon nanotube-based FEDs are characterized by superior display performances such as fast response time, wide viewing angles, wide operation temperatures, cathode ray tube (CRT) like colors, ultraslim features, low-cost, and low-power consumption. FED technology is one of the most promising approaches for direct view displays larger than 60-in. diagonal.[20] Research efforts are currently devoted to the in-situ growth of vertically aligned nanotubes over a large area of glass substrates at low temperatures. However, while MWNTs can be produced at relatively low temperatures, high synthesis temperatures are required to produce single-walled carbon nanotubes. In the latter case, the use of nanotubes produced separately and later deposited on the cathode by techniques such as the screen-printing method might be required.

In the present contribution, we report a comparative study of the field emission characteristics of CoMoCAT SWNTs still embedded in the silica-supported catalyst used in their synthesis. Researchers at Applied Nanotech Inc have recently shown that deposition of a mixture of nanotubes and dielectric nanoparticles leads to much improved emission characteristics.[21] This development makes a perfect combination with the high-quality single-walled carbon nanotubes (SWNTs) produced by the CoMoCAT catalytic method that we have developed.[22−29] The CoMoCAT product is particularly suitable for this application because it may be used in its as-prepared form, without elimination of the catalyst, given that its main component is silica (SiO_2), in the form of dielectric submicron particles. In the as-produced CoMoCAT product, SWNTs with controlled diameter distribution remain well dispersed and imbedded in the silica support in the form of bundles of different sizes, which can in turn be controlled by adjusting the synthesis parameters. It is important to compare the field emission (FE) parameters obtained from nanotubes with controlled structure and morphology and to compare these experimental values with available theoretical predictions[18,30−33] since such a direct comparison has not been previously done.

Experimental Section

Preparation of Materials. The SWNT used in this study were synthesized by the CoMoCAT method, described in previous publications.[22,23,28,29,34] Briefly, the silica-supported Co−Mo catalyst used in this method was prepared using cobalt nitrate and ammonium heptamolybdate as precursors in an aqueous impregnation method. The total metal loading was 2

* Author to whom correspondence should be addressed. Phone: 405-325-4370; fax: 405-325-5813; e-mail: resasco@ou.edu.

10.1021/jp0510488 CCC: $30.25
Published on Web 07/13/2005

wt % with a Co/Mo molar ratio of 1/3. Prior to the production of SWNT by the CO disproportionation reaction, the catalyst was heated in H_2 flow to 500 °C and then in He flow to the selected reaction temperature. CO disproportionation was carried out in a fluidized bed reactor in flow of pure CO at a total pressure of 80 Psi and at three different temperatures, 750, 850, and 950 °C. The as-produced (raw) nanotube/silica composites are denoted NTR750, NTR850, and NTR950, respectively. Because of the different synthesis temperatures, the surface area of the supported catalyst varies significantly. To determine the final surface area, without counting the surface area of the nanotubes, samples of the fresh catalysts were heated in He at the three different reaction temperatures. The resulting surface areas determined by BET were 98.2 m^2/g at 750 °C, 75.8 m^2/g at 850 °C, and 29.3 m^2/g at 950 °C.

Purified nanotube samples (NTP) from the different as-produced materials were also prepared. To produce these samples, the SWNT/silica composites were attacked with HF solution (49% HF) as described elsewhere.[35] This purification method results in the complete elimination of the silica support and most of the metal (i.e., residual metal about 2 wt %).

Nanotube Characterization. The as-produced NTR powder samples were characterized by Raman spectroscopy, optical absorption, and electron microscopy. The Raman spectra were obtained in a Jovin Yvon-Horiba Lab Ram equipped with a charge-coupled detector and with He−Ne laser (632 nm) as excitation source.

The morphology of the SWNT−silica composites was examined by electron microscopy (SEM and TEM). SEM images were obtained in a JEOL JSM-880 high-resolution scanning electron microscope while the TEM pictures were obtained in a JEOL JEM-2000FX transmission electron microscope. For this analysis, each NTR sample was dispersed in 2-propanol and ultrasonicated for 10 min. A few drops of the suspension were deposited on the TEM grid, then dried, and evacuated before analysis.

The nanotubes employed in this study were further characterized by optical absorption measurements in the wavelength range 400−1400 nm. Since this particular characterization must be conducted in liquid suspension, the NTP samples suspended in NaDDBS were used for this purpose. As we have previously shown,[35] NaDDBS is an effective surfactant to suspend CoMoCAT nanotubes. The resulting solution was ultrasonicated for 2 h and centrifuged at 15 000 rpm for 1.5 h. Then, the supernatant fraction was diluted in DI water and characterized by vis-NIR spectroscopy. The approximate concentrations of SWNT and surfactant in these suspensions were 0.15 and 3 mg/mL, respectively.

Field Emission Measurements. The field emission measurements were conducted in a simple diode setup and were placed in a vacuum chamber with $10^{-6}\sim10^{-7}$ Torr base pressure. The cathode and anode in the diode were separated by a ceramic spacer of well-controlled thickness (250 μm). For each measurement with the as-produced (NTR) material, the sample was ground to a very fine powder and was mixed with a conducting Ag-based fluro-elastomer binder to form the emitting film. The film was attached to the stainless steel cathode by a double-faced copper tape.

For the measurement of the purified sample (NTP), the SWNTs were suspended in the NaDDBS solution and were ultrasonicated for 10 min. The SWNT:surfactant weight ratio was kept at 1:2. The NaDDBS-based NTP suspension was then pressure-filtered through a 0.5-μm stainless steel frit. The SWNT-coated frit was attached to the cathode with a double-faced copper tape.

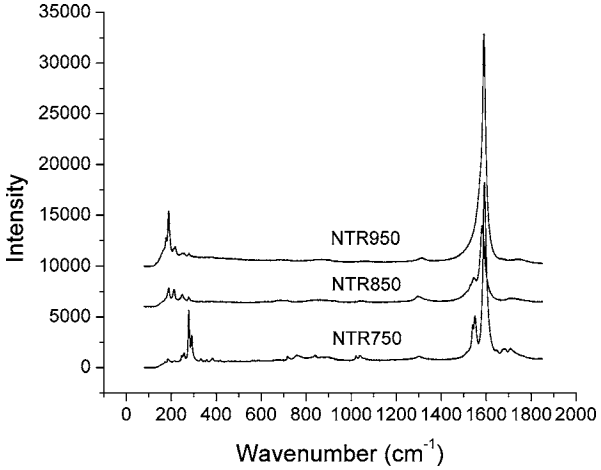

Figure 1. Raman spectra of as-produced SWNT/silica composites synthesized at 750, 850, and 950 °C. The wavelength of excitation laser is 633 nm.

The I−V curves were recorded using a Keithley 2410 sourcemeter. To investigate the field emission process, a sequential sweeping method was employed. In this method, the voltage is increased in a sequence of six different ranges: 1−100 V, 1−300 V, 1−500 V, 1−700 V, 1−900 V, and 1−1100 V. Each sweep was run twice to determine the irreversibility of the process. As a result, the sample in the last 1−1100 V cycle has been ramped 12 times.

Results

Raman spectroscopy is a widely used technique for characterizing SWNT samples and gaining information about their structure. Figure 1 presents the typical Raman spectra of the as-produced NTR material produced by the CoMoCAT method at 750, 850, and 950 °C.

The band appearing at about 1580 cm^{-1} (G band) results from the in-plane stretching mode of ordered crystalline graphitelike structures, while the band appearing at around 1340 cm^{-1} (D band) represents disordered carbon structure. Consequently, the quality parameter that we have previously defined (1-D/G) can be used as an approximate measure of the nanotube quality. In all the samples used in this study, the observed quality parameter was close to 1, which indicates that concentration of carbonaceous impurities or imperfections in carbon nanotubes was low in all samples. The series of bands in the range 150−400 cm^{-1} are associated with the radial breathing mode (RBM) and are characteristic of single-walled carbon nanotubes. As shown in Figure 1, the position of the intense RBM bands observed for NTR750, NTR850, and NTR950 samples vary with reaction temperature. As the temperature increases, the RBM bands shift to lower wavenumbers. As previously described,[34] this systematic shift is consistent with an increase in nanotube diameter as the synthesis temperature increases, since, as it is well-known, the frequency of the RBM is inversely proportional to the nanotube diameter.

Assignment of RBM bands to specific nanotube structures is not straightforward, and diameter populations obtained from RBM are not reliable unless a very detailed study is attempted. The dramatic effect of resonance phenomena, complicated by thermal effects and the effect of nanotube aggregation, can greatly alter the relative intensities of RBM bands.[36] Therefore, Raman results need to be complemented with an independent

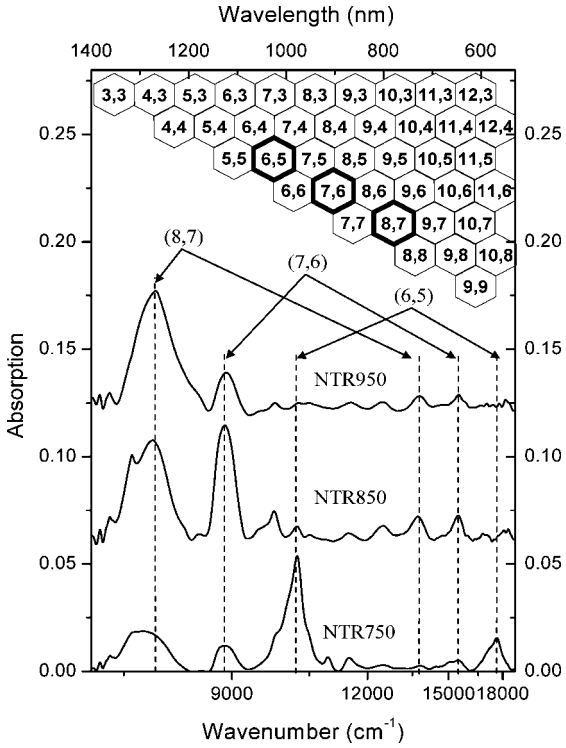

Figure 2. Optical absorption in visible-near-IR range for SWNT synthesized at different temperatures. Pure nanotubes suspended in NaDDBS solution (SWNT concentration 0.15 mg/mL, surfactant concentration 3 mg/mL). The most abundant species in samples produced at three temperatures are also located in the SWNT map at the top.

technique. Optical absorption is a very powerful technique that can be more quantitative than Raman in the assessment of nanotube populations. It is well-known that the quasi-one-dimensionality of SWNT gives origin to sharp van Hove singularities in the density of electronic states. As a result, the optical properties of SWNT are dominated by transitions between van Hove singularities on opposite sides of the Fermi level. Kataura[37] used the tight binding model to calculate energy transitions E_{ii} and generated the well-known Kataura plot of E_{ii} versus nanotube diameter, which is a function of the structural parameter (n,m). More recently, Weisman and Bachilo[38] have modified the Kataura plot on the basis of the photoluminescence (PL) method that they developed. This remarkable tool is particularly appropriate to characterize semiconducting nanotubes in the diameter range of those synthesized by our CoMoCAT method as recently shown.[22]

In this case, we have used optical absorption in the 400∼1400 nm range. The absorption spectra for the different nanotubes extracted from the NTR750, NTR850, and NTR950 by suspending them in NaDDBS surfactant are shown in Figure 2. Only a few sharp absorption peaks with a low background were obtained in the entire vis-NIR spectrum, in good agreement with previous PL results that evidenced the presence of few nanotube types, with similar diameter and chirality. With such a small number of nanotube types present in the sample, a detailed analysis and (n,m) assignment of the SWNT present in the sample is possible. By matching the corresponding E11 and E22 of the Weisman plot with the peak lines in the spectrum, it can be seen that a few semiconducting SWNTs dominate each of the NTR samples. Using a UV−vis spectrophotometer, it was observed that the bands corresponding to metallic SWNT are much weaker than those of the semiconducting nanotubes. However, since relative extinction coefficients of metallic and

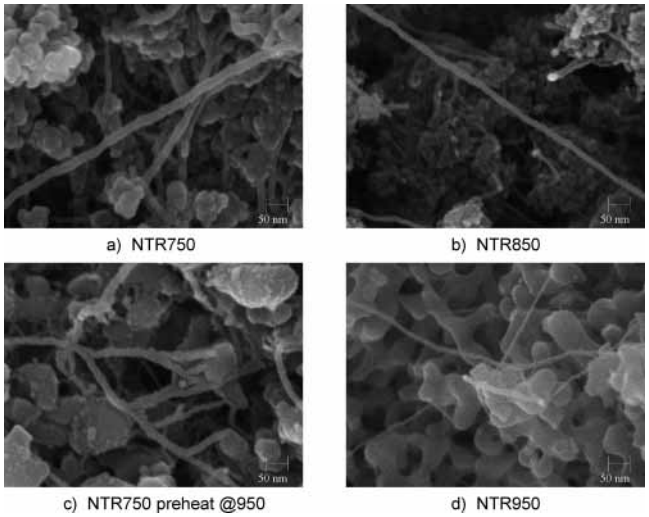

Figure 3. SEM images of SWNT/silica composites synthesized at different temperatures. (a) Composites produced at 750 °C, (b) composites produced at 850 °C, (c) composites produced at 750 °C after preheating at 950 °C, and (d) composites produced at 950 °C.

semiconducting nanotubes are not available, it is not possible to obtain from the spectra the metallic/semiconducting population ratio. Within the semiconducting nanotubes in the sample, the (6,5) type is the major constituent of NTR750 sample, while (7,6) dominates in NTR850 and (8,7) in NTR950. This trend is in agreement with the Raman results and previously reported TEM results that indicate that higher synthesis temperatures lead to SWNTs of larger diameter.[34] What is now more remarkable is that we can precisely identify the (n,m) types that dominate the nanotube population on the different samples.

In addition to the spectroscopic methods, SEM and TEM were utilized to directly observe the morphology of the different SWNT samples. Figure 3 shows SEM pictures for the three as-produced samples, NTR750, NTR850, and NTR950. Bundles of SWNTs are clearly seen meshing with the silica support particles in the three different samples. An interesting conclusion can be derived from the analysis of these images. It is consistently seen that the diameter of the nanotube bundles decreases as the reaction temperature increases. That is, the trend is the opposite to that observed regarding the diameter of each individual SWNT, which as shown above, increases with temperature. The estimated bundle size varies from 20 nm at 750 °C to 10 nm at 850 °C and to 5 nm at 950 °C. Evidently, when the reaction temperature increases to 950 °C not only the nanotubes, but also the silica support, exhibit a significant morphological change because of a severe thermal sintering. To determine whether the support sintering rather than the reaction temperature itself causes the decrease in bundle size, we conducted the following experiment. Before the nanotube growth step, the catalyst was preheated in He for 10 min at 950 °C, and then it was cooled to 750 °C, at which temperature the nanotube growth was conducted. As shown in Figure 3c, despite the pretreatment at 950 °C that caused the silica sintering, the bundle size resulting from the growth at 750 °C was essentially the same as that obtained at 750 °C, without previous heating. Therefore, it seems that not the pretreatment in He but rather the reaction temperature (i.e., under CO gas) determines SWNT diameter and bundle size. The TEM images shown in Figure 4 illustrate the morphology of the typical bundles present in each of the three samples.

Most previous field emission studies involving SWNT have employed purified nanotubes. By contrast, the as-produced

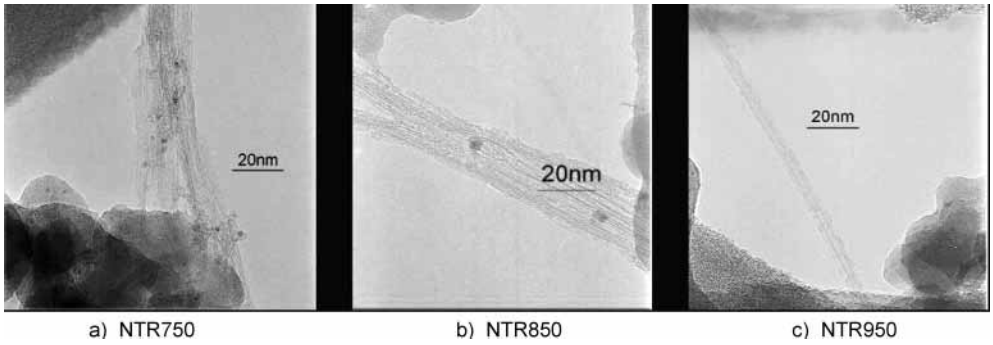

Figure 4. TEM images of SWNT/silica composites at different temperatures. (a) Composites produced at 750 °C, (b) composites produced at 850 °C, and (c) composites produced at 950 °C.

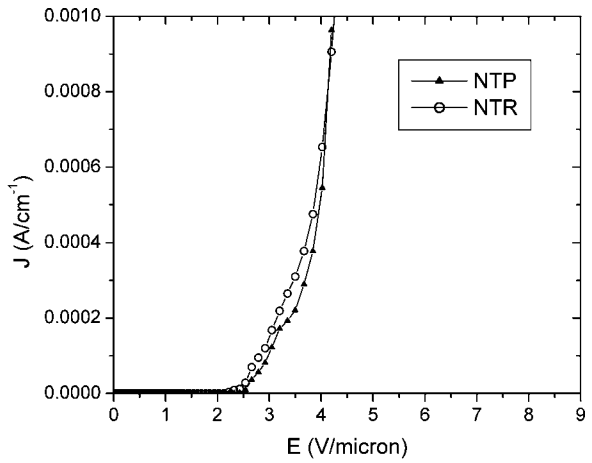

Figure 5. Emission current as a function of field from purified SWNT (NTP) and as-produced SWNT/silica composites (NTR).

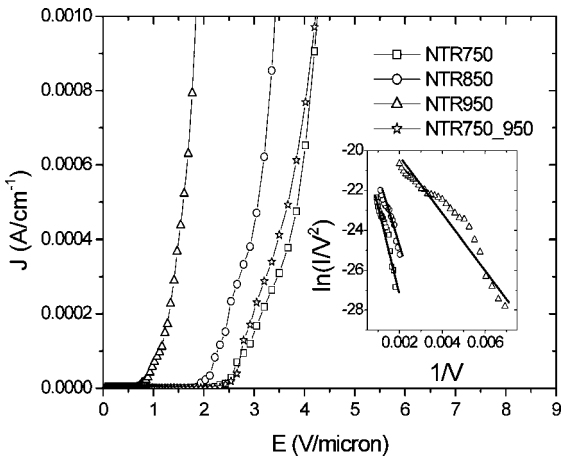

Figure 6. Emission current as a function of field from SWNT/silica composites (NTR) synthesized at different temperatures. Inset is the Fowler−Nordheim plot derived from field emission data of NTR750, NTR850, and NTR950.

SWNT material used in this study contains the original porous silica support and the catalytic metals. The practical importance of this modality arises from the possibility of using the as-produced material, thus avoiding the purification step. In this way, not only the cost of the material would be reduced but the potential damage of the nanotubes by the acid treatment is prevented. Figure 5 compares the field emission characteristics of the as-produced SWNT/silica composite (NTR750) with that of purified SWNT (denoted NTP). The SWNT content in the films is around 0.0003 and 0.011 mg/mm^3, respectively. The two curves demonstrate that the NTR has comparable electron emission characteristics as the NTP with a much lower SWNT density. One reason for the higher effective utilization of the nanotubes in the NTR samples could be the reduced shielding[17] because of the presence of the dielectric silica particles intermixed with the nanotubes as opposed to the densely entangled SWNT that are present in the purified film.

To investigate the field emission properties of the as-produced composites, we performed current−voltage measurements on the NTR750, NTR850, and NTR950 samples as well as on the composite synthesized at 750 °C after preheating in inert gas at 950 °C. Figure 6 compares the electron emission characteristics of the composites synthesized at different temperatures. A trend in extraction field with nanotube synthesis temperature is observed. NTR950, with the smallest bundle size but the largest nanotube diameter, has the lowest extraction field, 0.6 V/μm. This sample reaches the target of 1 mA/cm^2 at a field of 1.8 V/μm, showing the best emission performance among the three samples. While the other two samples, NTR850 and NTR750, also show very good field emission properties, the extraction fields for them was 1.6 and 2.2 V/μm, respectively, in a clear trend with the synthesis temperature; the field needed for generating the current density of 1 mA/cm^2 was 3.4 and 4.3 V/μm, respectively. In separate measurements, the maximum current density achieved with each sample was determined. In this case, it was observed that the maximum current density decreased with synthesis temperature; that is, the maximum values for NTR750, NTR850, and NTR950 were 13.7, 12.1, and 3.44 mA/cm^2, respectively. Thus, it appears that although increasing the synthesis temperature results in an improvement in extraction field it limits the maximum current density. Therefore, an intermediate synthesis temperature might be the optimal solution.

Discussion

By combination of Raman, electron microscopy, and optical absorption studies, we have shown that the SWNT/silica composites synthesized by the CoMoCAT process at different temperatures contain nanotubes of gradually different nanotube diameters and bundle sizes, from smaller diameter and larger bundles at lower temperatures (750 °C) to larger diameter and smaller bundles at higher temperatures (950 °C). This controlled trend has allowed us to investigate the effect of nanotube structure on the field emission characteristics of the as-produced SWNT/silica composites.

The detailed analysis of the optical absorption spectra has allowed us to identify the (n,m) identity of the most abundant nanotube components in each of the as-produced SWNT samples, for example, the most abundant semiconducting species in NTR750 is the (6,5) nanotube. As we have previously discussed in other contributions,[39] the increase in nanotube diameter with synthesis temperature can be explained by a faster

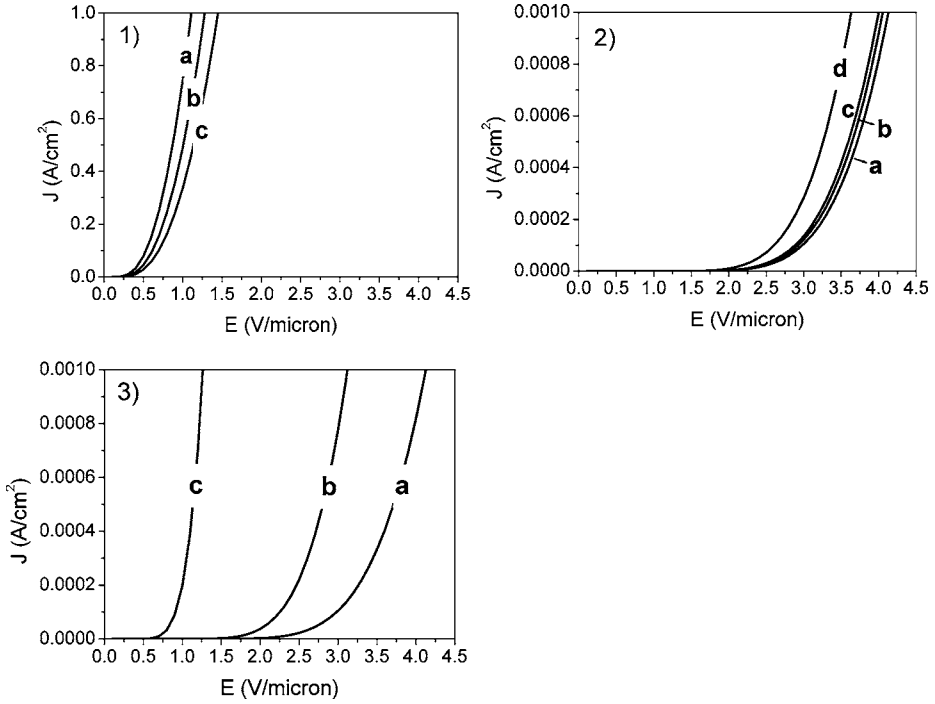

Figure 7. Simulated field emission with different assumptions. (1) The emitter size is the radius of the individual nanotube and the work function is the theoretical value [40] for each nanotube, i.e., (a) 5.24 eV for (6,5), (b) 5.16 eV for (7,6), and (c) 5.10 eV for (8,7); (2) the work functions are those characteristic of the (a) (6,5), (b) (7,6), (c) (8,7), and (d) (6,6) nanotubes, emitter size is constantly 20 nm for bundles composed of each type of tubes; (3) the emitters are (a) 20-nm bundle of (6,5), (b) 15-nm bundle of (7,6), and (c) 5-nm bundle of (8,7).

TABLE 1: Calculated Results from the Experimental Field Emission Data for NTR750, NTR850, and NTR950

	NTR750	NTR850	NTR950
$\ln(I/V2) = A(1/V) + B$	$A = -4449.3$ $B = -18.136$	$A = -3277.2$ $B = -18.28$	$A = -1307.2$ $B = -17.779$
theoretical work function ϕ (eV)	5.24	5.16	5.10
field enhancement factor β (cm^{-1})	184 658	244 282	601 775
size of emitter (nm)	22.3	15.8	5.6

growth of the cobalt clusters during the carbon nucleation period. That is, at higher temperatures, by the time carbon has nucleated to form the nanotube cap that determines the nanotube size, the Co cluster responsible for the growth of the nanotube has grown larger. At lower temperatures, the nucleation and cap formation occurs over Co clusters of smaller size. By contrast, the tendency to form smaller bundles at higher temperature is harder to explain. It is not clear to us at this point whether this is a general trend that is due to the nature of nanotube−nanotube interaction during the bundle formation and how it is affected by temperature or if it is a result of the variations in pore structure of the catalyst during the heating. A simple experiment that we conducted to investigate the effect of the support structure on the formation of bundle seems to indicate that this effect is not the most critical. Heating at 950 °C causes a significant drop in surface area and pore volume since the high-temperature pretreatment causes an irreversible sintering on the silica pore structure. However, when the catalyst was heated to 950 °C for 10 min and then cooled to 750 °C for the SWNT growth, the resulting bundle size was the same as that obtained without the preheating step.

One can expect that the changes in morphology and aggregation state that can be reproducibly obtained by our catalytic method should have an impact on the work function and other electrical characteristics that determine the field emission properties of composites.

From the well-known Fowler−Nordheim theory, the emission current density J can be written and simplified as[40]

$$J = 1.54 \times 10^{-6}\frac{E^2}{\phi}\exp\left[-6.83 \times 10^{7}\frac{\phi^{1.5}}{E}\right] \qquad (1)$$

where J is in A/cm^2, the electric field E is in V/μm, and the work function Φ is in eV. For plotting convenience, we use I and V to replace J and E, respectively, from the relations

$$J = \frac{I}{S} \qquad E = \beta V$$

where S is the emitting area, equal to 0.1926 cm^2 in our case, and β is the field enhancement factor that accounts for the geometry of the emitter. Different empirical formulas have been provided to calculate this factor. Here, we choose the paraboloid approximation

$$\beta = \frac{2}{r\ln(2R/r)} \qquad (2)$$

where R is the distance between the emitter tip and the anode

while r is the radius of curvature of the tip. By rearranging eq 1, we obtain

$$\ln(I/V^2) = -6.83 \times 10^7 \frac{\phi^{1.5}}{\beta} \times (1/V) + \ln\left(1.54 \times 10^{-6} \times S\frac{\beta^2}{\phi}\right) = A(1/V) + B \quad (3)$$

Thus, the F−N plots in the inset of Figure 6 can be fitted to eq 3 to calculate the parameter β and subsequently r.

It is widely accepted that the work function can be obtained from *IV*s. *V* curves only on those cases in which single emitters are being used. A more common practice has been to assume a given work function for the emitter and then calculating the parameter β. Some authors[41,42] have used work function values typical of graphite (i.e., about 5 eV). In this case, the fitting of the data in Figure 6 was conducted using the theoretical work functions of the most abundant species in each sample, that is, (6,5), (7,6), and (8,7). As shown below, the small variations in the work functions for the different nanotubes do not have a significant impact on the resulting extraction field values. Therefore, the only adjustable parameter resulting from the fitting is the field enhancement factor, from which the emitter size can be directly calculated. The resulting parameters are summarized in Table 1. The calculated emitter sizes for the different samples are in excellent agreement with the trend in bundle size observed experimentally by SEM. These results indicate that the geometrical factors that determine the field enhancement play a more important role in determining the extraction field in nanotube samples than differences in the work functions of the specific nanotubes present in the sample.

To further illustrate the influence of these two parameters, we have simulated $I-V$ emission curves for several hypothetical conditions. These simulated curves are depicted in Figure 7. The following cases are considered: (a) emission from individual SWNT, in which the emitter size is the radius of the individual nanotube and the work function is the theoretical value[43] for each nanotube, that is, 5.24, 5.16, and 5.10 eV for the (6,5), (7,6), and (8,7) nanotubes, respectively; (b) the work functions are those characteristic of the (6,5), (7,6), (8,7), and (6,6) (4.7 eV) nanotubes, respectively; the emitter size is considered fixed at 20 nm, representing bundles of the same size; (c) the work functions are those characteristic of the (6,5), (7,6), and (8,7) nanotubes, respectively; the emitter sizes are those observed in SEM and TEM pictures, that is, 20, 15, and 5 nm. Moreover, even for the metallic (6,6) nanotube which has a diameter close to those of the semiconducting (6,5), (7,6), and (8,7) nanotubes but a lower work function (4.7 eV), the field emission enhancement is very small compared to the one caused by differences in bundle size. Hence, it can be inferred that the greatest variation of field emission properties arise from differences in emitter size rather than differences in work function.

Conclusion

By using the highly selective CoMoCAT catalytic method, SWNT/silica composites have been synthesized with controlled diameter and bundle size, as characterized by Raman spectroscopy, optical absorption, SEM, and TEM. The vis-NIR optical absorption spectra were used to assign the (n,m) identification parameters to the most abundant nanotubes present on samples synthesized at various temperatures ranging from 750 to 950 °C. A simple analysis of the data suggests that the bundle size, rather than the nanotube diameter or differences in work function, is more important in determining the field emission properties of SWNT/silica composites. The possibility of tailoring the electrical properties of SWNT emitters by adjusting the synthesis parameters has been demonstrated. In addition, the present results show that the as-produced SWNT/silica composites have similar or perhaps better field emission properties than the purified nanotube samples, even though the concentration of nanotubes on the emitting surface of the as-produced was much lower than that in the pure SWNT sample. The good field emission efficiency of the as-produced material combined with the convenience of eliminating any purification process make this material an attractive field emitter.

Acknowledgment. The authors gratefully acknowledge the financial support from the Department of Energy (Grant DE-FG03-02ER15345) and from the National Science Foundation (Grant No. CTS-0308619).

References and Notes

(1) Wang, Q. H.; Corrigan, T. D.; Dai, J. Y.; Chang, R. P. H.; Krauss, A. R. *Appl. Phys. Lett.* **1997**, *70*, 3308.
(2) Deheer, W. A.; Chatelain, A.; Ugarte, D. *Science* **1995**, *270*, 1179.
(3) Rinzler, A. G.; Hafner, J. H.; Nikolaev, P.; Lou, L.; Kim, S. G.; Tomanek, D.; Nordlander, P.; Colbert, D. T.; Smalley, R. E. *Science* **1995**, *269*, 1550.
(4) Collins, P. G.; Zettl, A. *Appl. Phys. Lett.* **1996**, *69*, 1969.
(5) Bonard, J. M.; Maier, F.; Stockli, T.; Chatelain, A.; de Heer, W. A.; Salvetat, J. P.; Forro, L. *Ultramicroscopy* **1998**, *73*, 7.
(6) Bonard, J. M.; Salvetat, J. P.; Stockli, T.; de Heer, W. A.; Forro, L.; Chatelain, A. *Appl. Phys. Lett.* **1998**, *73*, 918.
(7) Bonard, J. M.; Salvetat, J. P.; Stockli, T.; Forro, L.; Chatelain, A. *Appl. Phys. A* **1999**, *69*, 245.
(8) Bonard, J. M.; Kind, H.; Stockli, T.; Nilsson, L. A. *Solid-State Electron.* **2001**, *45*, 893.
(9) Bonard, J. M.; Croci, M.; Klinke, C.; Kurt, R.; Noury, O.; Weiss, N. *Carbon* **2002**, *40*, 1715.
(10) Yuan, Z. H.; Huang, H.; Dang, H. Y.; Cao, J. E.; Hu, B. H.; Fan, S. S. *Appl. Phys. Lett.* **2001**, *78*, 3127.
(11) Zhou, G.; Duan, W. H.; Gu, B. L. *Phys. Rev. Lett.* **2001**, *8709*, 095504.
(12) Jo, S. H.; Tu, Y.; Huang, Z. P.; Carnahan, D. L.; Wang, D. Z.; Ren, Z. F. *Appl. Phys. Lett.* **2003**, *82*, 3520.
(13) Umnov, A. G.; Matshushita, T.; Endo, M.; Takeuchi, Y. *Chem. Phys. Lett.* **2002**, *356*, 391.
(14) Jo, S. H.; Tu, Y.; Huang, Z. P.; Carnahan, D. L.; Huang, J. Y.; Wang, D. Z.; Ren, Z. F. *Appl. Phys. Lett.* **2004**, *84*, 413.
(15) Zhou, G.; Duan, W. H.; Gu, B. L. *Appl. Phys. Lett.* **2001**, *79*, 836.
(16) Bonard, J. M.; Dean, K. A.; Coll, B. F.; Klinke, C. *Phys. Rev. Lett.* **2002**, 89.
(17) Feng, Y. T.; Deng, S. Z.; Chen, J.; Xu, N. S. *Ultramicroscopy* **2003**, *95*, 93.
(18) Liang, S. D.; Xu, N. S. *Appl. Phys. Lett.* **2003**, *83*, 1213.
(19) Choi, W. B.; Chung, D. S.; Kang, J. H.; Kim, H. Y.; Jin, Y. W.; Han, I. T.; Lee, Y. H.; Jung, J. E.; Lee, N. S.; Park, G. S.; Kim, J. M. *Appl. Phys. Lett.* **1999**, *75*, 3129.
(20) Sato, F.; Seki, M. *Proceedings of Asia Display/IDW'01*, Nagoya, Japan, 2001.
(21) Mao, D. S.; Fink, R. L.; Monty, G.; Thuesen, L.; Yaniv, Z. *Proceedings of 9th International Display Workshops/IDW'02*, Hiroshima, Japan, 2002.
(22) Bachilo, S. M.; Balzano, L.; Herrera, J. E.; Pompeo, F.; Resasco, D. E.; Weisman, R. B. *J. Am. Chem. Soc.* **2003**, *125*, 11186.
(23) Resasco, D. E.; Alvarez, W. E.; Pompeo, F.; Balzano, L.; Herrera, J. E.; Kitiyanan, B.; Borgna, A. *J. Nanopart. Res.* **2002**, *4*, 131.
(24) Alvarez, W. E.; Pompeo, F.; Herrera, J. E.; Balzano, L.; Resasco, D. E. *Abstr. Pap.—Am. Chem. Soc.* **2002**, *223*, U630.
(25) Alvarez, W. E.; Pompeo, F.; Herrera, J. E.; Balzano, L.; Resasco, D. E. *Chem. Mater.* **2002**, *14*, 1853.
(26) Herrera, J. E.; Balzano, L.; Borgna, A.; Alvarez, W. E.; Resasco, D. E. *J. Catal.* **2001**, *204*, 129.
(27) Alvarez, W. E.; Kitiyanan, B.; Borgna, A.; Resasco, D. E. *Carbon* **2001**, *39*, 547.

(28) Resasco, D. E.; Kitiyanan, L.; Alvarez, W. E.; Borgna, A. *Abstr. Pap.— Am. Chem. Soc.* **2000**, *219*, U536.
(29) Kitiyanan, B.; Alvarez, W. E.; Harwell, J. H.; Resasco, D. E. *Chem. Phys. Lett.* **2000**, *317*, 497.
(30) Liu, X.; Pichler, T.; Knupfer, M.; Fink, J.; Kataura, H. *Phys. Rev. B* **2004**, 69.
(31) Mayer, A.; Miskovsky, N. M.; Cutler, P. H. *J. Vac. Sci. Technol., B* **2003**, *21*, 395.
(32) Mayer, A.; Miskovsky, N. M.; Cutler, P. H. *J. Phys.: Condens. Matter* **2003**, *15*, R177.
(33) Mayer, A.; Miskovsky, N. M.; Cutler, P. H. *J. Vac. Sci. Technol., B* **2003**, *21*, 1545.
(34) Herrera, J. E.; Balzano, L.; Pompeo, F.; Resasco, D. E. *J. Nanosci. Nanotechnol.* **2003**, *3*, 133.
(35) Matarredona, O.; Rhoads, H.; Li, Z. R.; Harwell, J. H.; Balzano, L.; Resasco, D. E. *J. Phys. Chem. B* **2003**, *107*, 13357.
(36) Heller, D. A.; Barone, P. W.; Swanson, J. P.; Mayrhofer, R. M.; Strano, M. S. *J. Phys. Chem. B* **2004**, *108*, 6905.
(37) Kataura, H.; Kumazawa, Y.; Maniwa, Y.; Umezu, I.; Suzuki, S.; Ohtsuka, Y.; Achiba, Y. *Synth. Met.* **1999**, *103*, 2555.
(38) Weisman, R. B.; Bachilo, S. M. *Nano Lett.* **2003**, *3*, 1235.
(39) Herrera, J. E.; Resasco, D. E. *J. Phys. Chem. B* **2003**, *107*, 3738.
(40) Purcell, S. T.; Binh, V. T.; Baptist, R. *J. Vac. Sci. Technol., B* **1997**, *15*, 1666.
(41) Kang, D. W.; Suh, J. S. *J. Appl. Phys.* **2004**, *96*, 5324.
(42) Sun, J. P.; Zhang, Z. X.; Hou, S. M.; Zhang, G. M.; Gu, Z. N.; Zhao, X. Y.; Liu, W. M.; Xue, Z. Q. *Appl. Phys. A* **2002**, *75*, 479.
(43) Zhao, J. J.; Han, J.; Lu, J. P. *Phys. Rev. B* **2002**, 65.